Molecular BioSystems
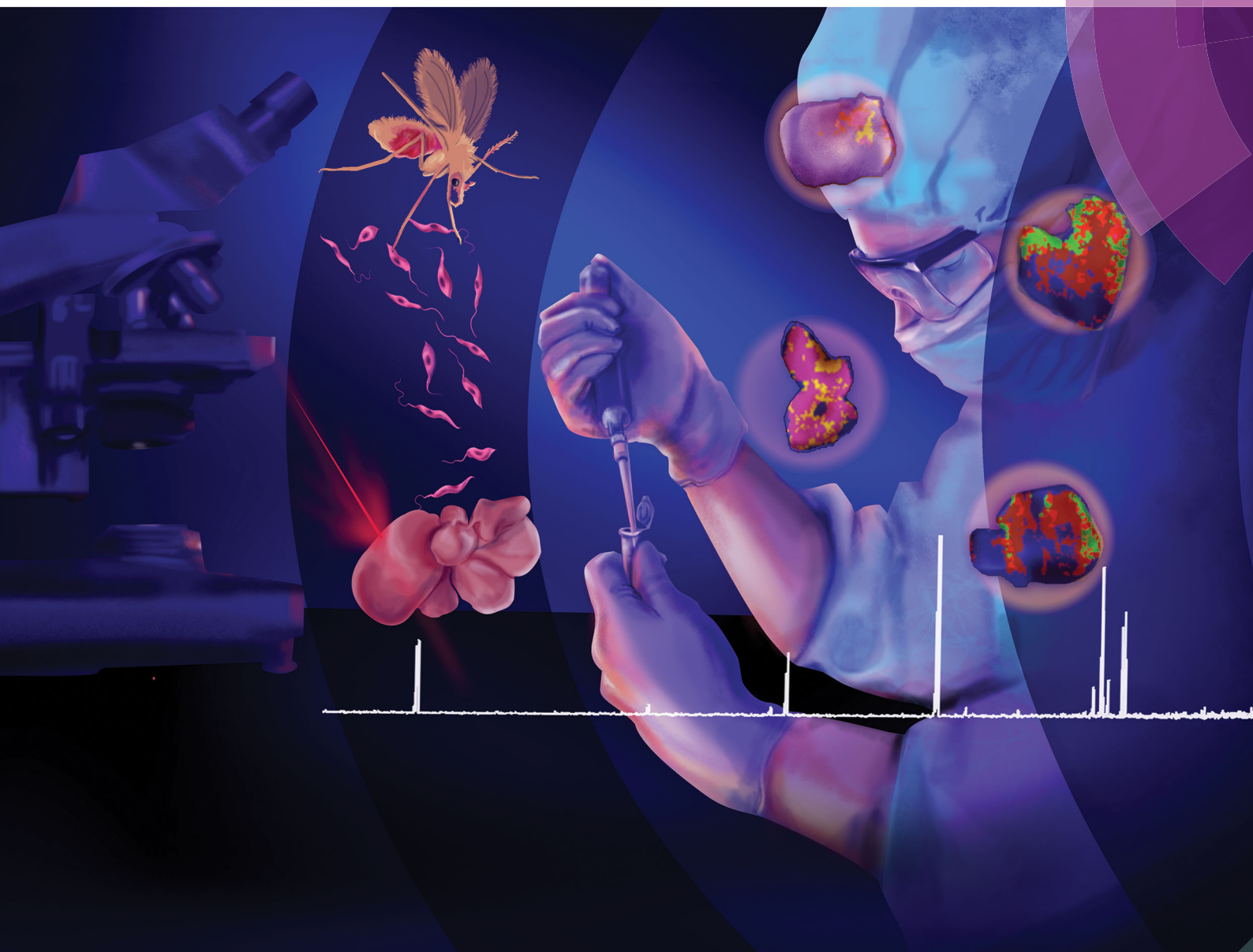
Interfacing chemical biology with the -omic sciences and systems biology

rsc.li/molecular-biosystems

ROYAL SOCIETY OF CHEMISTRY

PAPER
D. F. O. Rocha *et al.*
MALDI MS imaging investigation of the host response to visceral leishmaniasis

Indexed in Medline!

Check for updates

MALDI MS imaging investigation of the host response to visceral leishmaniasis†

C. F. Jaegger,[a] F. Negrão, [a] D. M. Assis,[b] K. R. A. Belaz,[a] C. F. F. Angolini, [a] A. M. A. P. Fernandes,[a] V. G. Santos,[a] A. Pimentel,[c] D. R. Abánades,[c] S. Giorgio,[c] M. N. Eberlin[a] and D. F. O. Rocha [a]*[a]

Mass spectrometry imaging (MSI) of animal tissues has become an important tool for *in situ* molecular analyses and biomarker studies in several clinical areas, but there are few applications in parasitological studies. Leishmaniasis is a neglected tropical disease, and experimental mouse models have been essential to evaluate pathological and immunological processes and to develop diagnostic methods. Herein we have employed MALDI MSI to examine peptides and low molecular weight proteins (2 to 20 kDa) differentially expressed in the liver during visceral leishmaniasis in mice models. We analyzed liver sections of Balb/c mice infected with *Leishmania infantum* using the SCiLS Lab software for statistical analysis, which facilitated data interpretation and thus highlighted several key proteins and/or peptides. We proposed a decision tree classification for visceral leishmaniasis with distinct phases of the disease, which are named here as healthy, acute infection and chronic infection. Among others, the ion of *m/z* 4963 was the most important to identify acute infection and was tentatively identified as Thymosin β4. This peptide was previously established as a recovery factor in the human liver and might participate in the response of mice to *Leishmania* infection. This preliminary investigation shows the potential of MALDI MSI to complement classical compound selective imaging techniques and to explore new features not yet recognized by these approaches.

Introduction

Mass spectrometry imaging (MSI) has been established as a new and efficient tool to understand the molecular process of disease progression as well as to find new biomarker candidates. MSI allows the exploration of all kinds of biomolecules from a tissue surface in a non-selective and label-free approach, with no previous information about such molecules. The usual strategy is to compare specific pathological conditions with healthy conditions hoping to identify under- or overexpressed biomolecules. There are several MS ionization techniques suitable for MSI, however, only matrix assisted laser desorption ionization (MALDI) enables intact protein ionization usually followed by detection *via* time of flight (TOF) mass spectrometry.[1–3] The huge amount of data generated by MSI requires careful data

treatment and statistical analysis, since important features could be ignored by visual inspection, as well as wrong assumptions could be made.[4] Considering the efficacy so far demonstrated by MSI to reveal new disease-related biomolecules,[1,5–8] including infection models,[5,9] its application in parasitic diseases should be explored.

Leishmaniasis is a neglected disease transmitted by bites of female phlebotomine infected with *Leishmania*. Promastigotes are flagellar forms localized in the sandflies' proboscis inoculated into the skin during the blood meal and phagocytosed mainly by macrophages. They subsequently differentiate into amastigote forms and replicate (revised by Arango Duque & Descoteaux, 2015[10]). The clinical symptoms vary from cutaneous lesions to chronic visceral injuries, depending on the parasite species and the immune status of the patient.[11] In Latin America, visceral leishmaniasis is mainly caused by *L. infantum* and is associated with fever, weight loss and enlargement of the spleen and liver.[12] *L. infantum* is also the most common cause of canine leishmaniasis worldwide.[13] Diagnosis of visceral leishmaniasis relies on the direct finding of parasites either in smears or in cultures from spleen or bone marrow aspirates, and there are few drugs and no human vaccine available.[14] Many animal experimental models have been developed to better understand parasite and host factors involved in the resistance and pathogenesis of

[a] ThoMSon Mass Spectrometry Laboratory, University of Campinas – UNICAMP, Campinas, SP, Brazil. E-mail: drocha@iqm.unicamp.br

[b] Bruker Daltonics, Atibaia, SP, Brazil

[c] Department of Animal Biology, Biology Institute, University of Campinas – UNICAMP, Campinas, SP, Brazil

† Electronic supplementary information (ESI) available: AIC trace for component selection, MALDI-TOF-MS spectra of the *L. infantum in vitro* culture and infected tissues, and the spatial distribution and intensity boxplot of the most differentially detected ion of *m/z* 4963. See DOI: 10.1039/c7mb00306d

Leishmania infection. Chronic visceral leishmaniasis can be experimentally established in mice by the inoculation of *L. infantum* amastigotes or promastigotes; in Balb/c mice it is non-fatal and the tissue pathology shows a similarity to the spectrum of clinical symptoms reported in human visceral leishmaniasis.[15] In the liver, *L. infantum* multiply and persist for months; innate and adaptive immune responses are induced during visceral leishmaniasis, and infiltrating inflammatory cells and granulomas are associated with liver chronic infection.[16]

Recently, MALDI-MS fingerprinting was used to identify *Leishmania* promastigotes at the species level, the insect form of this parasite maintained in cultures.[17] Regarding infected tissues, imaging techniques, mainly microscopy, have been extensively used to understand the complex relationship between *Leishmania* and the mammalian infected tissues and cells.[18] To the best of our knowledge, however, MSI has not yet been explored in mammalian infected cells or tissues. Aiming to investigate therefore the potential of MALDI MSI to reveal the profiles of peptides and proteins associated with visceral leishmaniasis, here we used this technique to study liver tissue from infected mice with different times post-infection (p.i.). Statistical analysis was also used to guide data interpretation and to select ions that might be related with the host response to parasite infection and tissue damage.

Experimental

Parasites, animals and evaluation of *L. infantum* infection

For experimental infection, female Balb/c mice (6 weeks of age) were injected intraperitoneally with 10^7 *L. infantum* amastigotes (MHOM/BR/1972/LD). All animal experiments were performed according to the principles stated in the Brazilian law on animal experiments and were approved by the UNICAMP Committee for Ethics in Animal Research (Protocol 4140-1). The investigation conforms with the Guide for the Care and Use of Laboratory Animals published by the Association for Assessment and Accreditation of Laboratory Animal Care (AAALAC International) and the Brazilian Guide for care and use of animals for scientific and didactic purposes (DBCA). For the determination of hepatic parasite burden, the liver was removed, weighed, cut into pieces and homogenized in Schneider medium.[19] The cells were diluted and amastigotes were counted in a Neubauer chamber. Fragments of the liver tissue were also fixed in 10% buffered formalin and embedded in paraffin blocks where the tissue sections (5 μm) were stained with hematoxylin–eosin. Impression smears were prepared and stained with Giemsa. The images were captured using a light microscope (a Carl Zeiss Primo Star model) and a camera (Axiocam model ERc5s).

Cell cultures

The J774 murine macrophage cell line was maintained in RPMI medium containing 10% (vol/vol) fetal bovine serum and gentamicin (50 μg mL^{-1}). J774 macrophages were distributed in 6-well culture plates and were infected by adding a suspension of living *L. infantum* promastigotes to the cell cultures in RPMI medium with a 20-fold excess of parasites for 16 h. The cell cultures were washed with PBS and trypsinized to remove non-internalized parasites. Amastigotes were obtained by culturing stationary phase promastigotes in Schneider's medium (pH was adjusted to 5.5 with succinic acid) at a temperature of 32 °C. Transformation was observed after 6 days of culture.

MALDI MSI

Samples. A frozen mouse liver was sliced into 14 μm tissue samples using a Cryotome (Leica Microsystems, Bannockburn, IL, USA) from Tissue-Tek (VWR International, Suwanee, GA, USA) as an optimal cutting temperature compound. A slice of each infection time was placed onto a conductive indium tin oxide (ITO) coated glass slide (BrukerDaltonics, Billerica, MA). Sequential 30 s washes were performed in 70, 90 and 95% ethanol, and the samples were dried in desiccators for 5 min. An α-cyano-4-hydroxycinnamic acid matrix (CHCA, Sigma) (40 mg in 40 mL acetonitrile/water 1 : 1 containing 2.5% of trifluoroacetic acid) was applied on the glass slide using a glass reagent sprayer.

Data acquisition. MALDI-TOF MS analysis was performed using a Bruker Autoflex III, equipped with Smartbeam™ laser technology (Bremem, Germany), and the chemical images were obtained through the Flex Control 3.4/Flex Imaging 4.0 software package (Bruker Daltonics, Bremen, Germany). MS data were acquired in linear positive ion mode in a mass range of *m/z* 2000–20 000 by 1000 consecutive laser shots in each pixel at a spatial resolution of 200 μm.

Data analysis. Data analysis and image generation were carried out using the FlexImaging 4.0 (Bruker Daltonics, Bremen Germany) and SCiLS Lab package software (SCiLS, Bremen Germany). For the import to SCiLS Lab, the original preprocessed data of one experiment was resampled to a number of 10 000 *m/z* bins. In all datasets, the interval width was set to ±5 *m/z* units. This *m/z* shift was chosen due to previous observed shifts in conducted imaging experiments. Each dataset was processed running the so-called preprocessing pipeline performing baseline subtraction. The total ion current (TIC) of each spectrum was used for the normalization of the ion signal intensity and the generation of one overview spectrum. Subsequently, MS ion peak picking was performed on the raw data and loaded and reduced to 8000 points per spectrum and to an automatic number of peaks per spectrum. The peak alignment was also performed on the mean spectra of the datasets to compensate the effect of slight misalignment between *m/z* values, and 1000 ion peaks were selected by modeling the mean spectra as a sum of ion peaks of the Gaussian shape plus noise, as described by Alexandrov *et al.* in 2010.[20] Relevant ion peaks were identified manually, considering adequate distribution over the entire area. Spatial segmentation was carried out by bisecting *k*-means, working on an individual spectrum with a correlation distance as well as a random initialization probabilistic latent semantic analysis (pLSA) with 5 components. In addition, we used a receiver operating characteristic

(ROC) curve to find discriminating masses, principal component analysis (PCA) and co-localization tools. The reduction of the spectrum-to-spectrum variation was accomplished by edge preserving spatial denoising, which was performed prior to segmentation.

Spatial segmentation. For the unsupervised mining of the datasets, spatial segmentation was employed by clustering the spectra into distinct groups as per their similarities. For the clustering process, the "bisecting k-means method" was selected, which is optimized for hierarchical clustering of large MALDI MSI datasets to find hidden structures in the unlabeled data. The number of clusters needed was defined by the histological experiments looking for recursive partitions in the data into two clusters at each step. Hence, the clustering process was conducted with the following parameters: for cluster initialization the farthest distance, and for the distance metrics the correlation distance were used. All described steps were carried out within the "segmentation pipeline" of the SCiLS Lab software.

pLSA. Probabilistic latent semantic analysis (pLSA) was also used as a multivariate analysis, where both score images and loadings can be interpreted in terms of mass spectra intensities. The results of the pLSA were therefore interpreted as spatial tissue components and their corresponding m/z distributions in the tissue. The optimal number of pLSA components for analysis was estimated in advance by the number of different visible histological distribution patterns of the liver on the course of *L. infantum* infection in Balb/c mice and by testing different numbers of components. Seven components turned out to be the best regarding the mentioned specified quality criteria and therefore used for all pLSA analysis. An AIC trace was carried out after exporting the data set from FlexImaging 4.0 to ClinProTools software (Bruker Daltonics, Bremen, Germany).

ROC. We used the receiver operating characteristic (ROC) tool[21–24] to check how discriminating some m/z values are between uninfected and infected tissues using SCiLS Lab. It is a univariate measure quantifying how well a selected m/z-value discriminates two different states. The calculation of an ROC for one m/z value involves estimating sensitivity and specificity m/z values for a trivial threshold classifier and then plotting a curve for the computed values. The area under the ROC curve (AUC value) assumes values between 0 and 1 and expresses the discrimination power of the m/z-signal in one value. A perfect discrimination would yield an AUC value equal to 1 (discrimination for group 1) or 0 (discrimination for group 2).

Co-localization. A co-localization step was carried out using the SCiLS Lab software by calculating the Pearson correlation between the spatial mask given by the selected masses and the intensities of an m/z-signal image of the tissue samples. The Pearson correlation coefficient quantifies the similarity between two m/z-images and takes values in the range from -1 to $+1$. While a value of $+1$ describes a perfect co-localization, a value of -1 characterizes a perfect anti-correlation, indicating that the m/z-images have an opposite localization. A value of 0 implies that there is no correlation detected between the two considered m/z-images.[25,26]

Bottom-up proteomics

Data acquisition. For protein analysis, an aliquot of 4.5 µL of proteins resulting from peptide digestion was separated by C18 (100 mm × 6100 mm) RP-nanoUPLC (nanoAcquity, Waters) coupled with a Q-Tof Premier mass spectrometer (Waters) using an nanoelectrospray source at a flow rate of 0.6 mL min^{-1}. The gradient was 2–90% acetonitrile in 0.1% formic acid over 20 min. The nanoelectrospray voltage was set to 3.5 kV, the cone voltage was 30 V and the source temperature was 100 °C. The instrument was operated in the 'top three' mode, in which one MS spectrum is acquired followed by MS/MS of the top three most intense ion peaks detected. After MS/MS fragmentation, the ion was placed on the exclusion list for 60 s and for the analysis of endogenous cleavage peptides, real-time exclusion was used.

Data analysis. The spectra were acquired using the MassLynx v.4.1 software and the raw data files were converted to a peak list format (mgf) without summing the scans by the software Mascot Distiller v.2.3.2.0, 2009 (Matrix Science Ltd) and searched against SwissProt 57.15 (515203 sequences; 181334896 residues, taxonomy *Mus musculus* (house mouse), 16230 sequences, 19 May 2016) using Mascot engine v.2.3.01 (Matrix Science Ltd), with carbamidomethylation as a fixed modification, the oxidation of methionine as a variable modification, one trypsin missed cleavage and a tolerance of 0.1 Da for both precursor and product ions.

Results and discussion

The infection in mouse livers was monitored every 30 days through the analysis of the liver morphology (macroscopic analysis) and through histological analysis of tissue sections (microscopic analysis), which allows us to monitor the infection kinetics. Hepatomegaly occurred at different times, early in the infection at 30 days post infection (p.i.) and 60 and 90 days p.i. The mouse livers at 30 days p.i. have a higher weight than the mouse livers at 60 and 90 days p.i. The parasite load was high at 30 and 60 days p.i., decreased by 90 days p.i., and was maintained at the same number (about 2×10^7 amastigotes per liver) in mice at 120 days p.i. (Fig. 1A). No parasite clearance was observed, confirming the aspect of chronic infection with *L. infantum*.[16] Inflammatory cell infiltrates, parasites and diffuse granulomas were observed in the liver at all time points (Fig. 1A and B). Our results are consistent with previously reported data.[27,28] Based on the number of parasites, liver weight, and macroscopic and microscopic analyses, we could therefore split infection into three distinct phases: healthy, acute infection (30 days) and chronic infection (60 and 90 days). Micro- and macroscopic analysis revealed that infected livers show different weights and the total number of parasites at the different times p.i. (Fig. 1). These differences corroborate with the statistical results provided below.
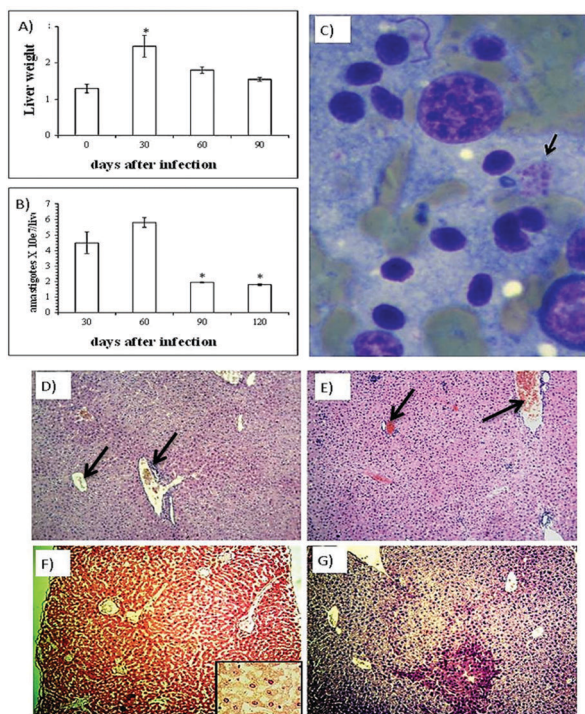
Fig. 1 Evaluation of the liver in the course of *L. infantum* infection in Balb/c mice. (A) The liver weights. (B) The total number of amastigotes per liver. (C) Impression smear of the mouse liver at 60 days p.i.; the arrow indicates amastigotes (1000×). (The results represent two independent experiments each including at least 3 mice per time point. *$P < 0.05$ is a statistically significant difference between mouse groups). Histology of the liver in the course of *L. infantum* infection in Balb/c mice. (D) Liver from an uninfected mouse with a normal histological aspect. The picture is mainly composed by hepatocytes (purple area) and blood vessels (arrows). (E) The liver from an infected mouse at 30 days p.i. showing defense cell infiltrates (spread dark purple dots) and monocyte recruitment (inside blood vessels there is an enlarged reddish region compared to the control tissue that indicates monocyte recruitment). (F) The liver from an infected mouse at 60 days p.i. showing defense cell infiltrates and necrosis almost extended to the whole tissue (100×); the inset shows damaged cells (1000×). (G) The liver from an infected mouse at 90 days p.i. showing defense cell infiltrates (spread dark purple dots), necrosis and granulomas where the purple area is more intense and agglomerated (100×). Hematoxylin–eosin stain; original magnification (×100).

MALDI-MSI and statistical analysis

The data set was loaded into the SCiLS software platform and processed for both spatial segmentation analysis[29] and pLSA[30,31] to allow data-dependent visualization of histological regions and to understand the changes in the liver protein profile detected in the macro- and microscopic analyses. The MS spectra were acquired with a lateral resolution of 200 μm and the laser focus diameter adjusted to 100 μm, and each spectrum covered the *m/z* 2000–20 000 range (Da if charge is 1+), and spatial segmentation analysis (Fig. 2A) statistically suggested 6 clusters per spectral similarity of the protein profile. All spectra of a particular cluster were then assigned a selected color and displayed as a spatial segmentation map in which all pixels are color-coded according to their cluster assignments. The blue cluster corresponds to the whole uninfected tissue indicating its relationship with the
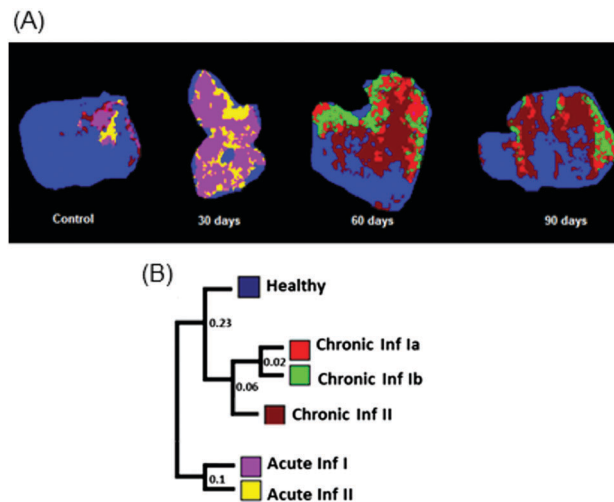

Fig. 2 Segmentation map analysis. (A) Area distribution (colors) per spectral similarity and (B) the dendrogram with the respective correlation distances (numbers) and color coded. Analysis was carried out by the "bisecting *k*-means method".

uninfected liver. Blue areas could be found not only in the control experiment but also in experiments of 60 days and in a bigger area in 90 days. Interestingly, the purple and yellow areas are found in the healthy tissue and by looking at the microscopic analysis, these areas contain agglomerates of defense cell (mostly neutrophils and monocytes). The reason for this is unknown and might be related to an uncertain metabolic dysfunction of the mouse. According to the dendrogram and correlation distances proposed by the segmentation map (Fig. 2B), the 30 days p.i. region was separated into two different clusters (purple and yellow) and showed no correlation with the healthy area. Based on the microscopic and macroscopic characteristics of the tissue, we defined the tissue at 30 days p.i. as an acute infection phase. We named therefore these 2 distinct regions as acute infection I and II. The regions originating from 60 and 90 days showed a correlation with the healthy area and were separated into 3 more closely correlated areas. Chronic infection was also confirmed by macroscopic and microscopic analyses of these regions. We named these clearly visualized regions as chronic infection Ia (red); chronic infection Ib – (green) and chronic infection II (brown). The levels selected in the segmentation dendrogram allowed – for the first time – the delineation of the distinct areas of the disease that microscopic analysis failed to discriminate in our experiments.

To address the same question in a different manner, random initialization probabilistic latent semantic analysis (pLSA) was proposed for the same data set. pLSA was first reported to treat the MS data in 2008,[32] and the advantage of this technique is to mainly differentiate cell types by *m/z* profile changes if it is present in varying proportions in the tissue. Even if the IMS spatial resolution is unable to resolve single cells, pLSA allows conclusions regarding individual tissue types and their respective MS data.

This ability is particularly interesting in human visceral leishmaniasis since the infected liver has a heterogeneous population of cells showing hyper cellularity, inflammatory

cellular infiltrates, parasites, diffuse granulomas and healthy tissue. For pLSA calculations, the number of components must be estimated by the user in advance. Given the heterogeneity and high complexity of infected liver cells, the number of components is unknown. Different numbers of components were tested repeating the analysis with different components and comparing the visual spectral quality. It was also checked by an automated estimation, called Akaike information criterion (AIC).[33] A total of 7 components (Fig. S1, ESI†) turned out therefore to be the best number regarding the parameters mentioned above.

Fig. 3 shows the distribution of pLSA scores for the healthy tissue and 30, 60 and 90 days p.i, and a total of seven components were assigned. Healthy tissue is described by component 1, a small area in the uninfected tissue, and component 2, which is spread in the uninfected and extremities in the infected tissues. Acute infection I and II are then described by components 3 and 4, respectively. These areas have different sizes in the 30 days p.i. tissue and are the complementary regions. Finally, chronic infection Ia, Ib and II is described by components 5, 6 and 7, respectively, and is located in the 60 and 90 days p.i. tissues. Components 5 and 6 are peripheric areas, whereas component 7 represents the central and biggest area. Fig. 1 shows microscopic analysis which reveals similar events at all times p.i., but some highlights are more characteristic depending on the stage of

infection. Inflammatory cellular infiltrates were detected especially at 30 days p.i (components 3 and 4); granulomas, and coagulative and liquefactive necrosis were detected at 60 and 90 days p.i. (components 5, 6 and 7). Normal hepatocytes are more abundant in the healthy tissue (components 1 and 2).

These results are in concordance with spatial segmentation where combined components 1 and 2 are related to the blue cluster (healthy), component 3 to the purple region (acute infection I), component 4 to the yellow region (acute infection II), component 5 to the red region (chronic infection Ia), component 6 to the green region (chronic infection Ib) and component 7 to the brown region (chronic infection II). Fig. 4 also shows pLSA loadings which are represented as reconstructed mass spectra. The results of pLSA can therefore be interpreted as the mass spectra specific for each phase or each histological condition compared to the uninfected and infected liver in different stages of infection. This result indicates
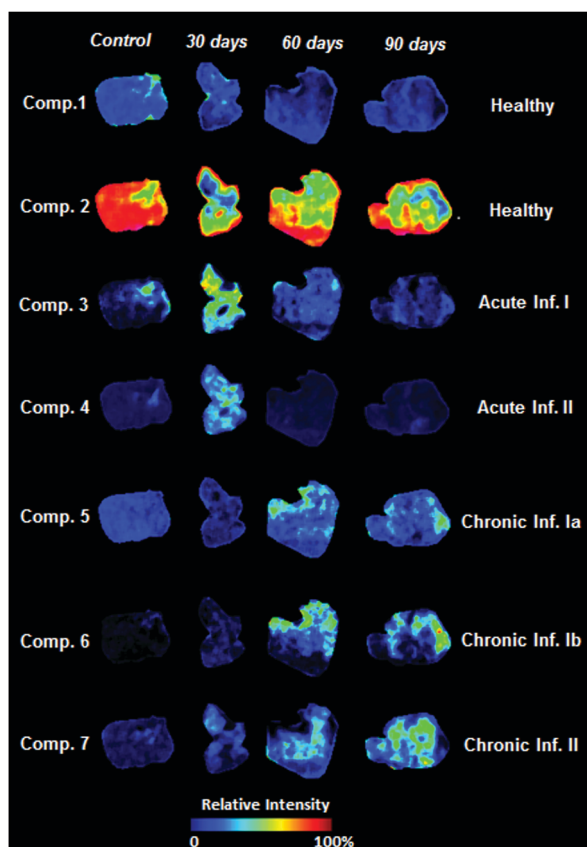

Fig. 3 pLSA components for an *L. infantum* infected liver applied to the MALDI MSI dataset, visualized using SCiLS Lab. The color scale represents the pattern distribution of the relative intensity of peaks for each component.
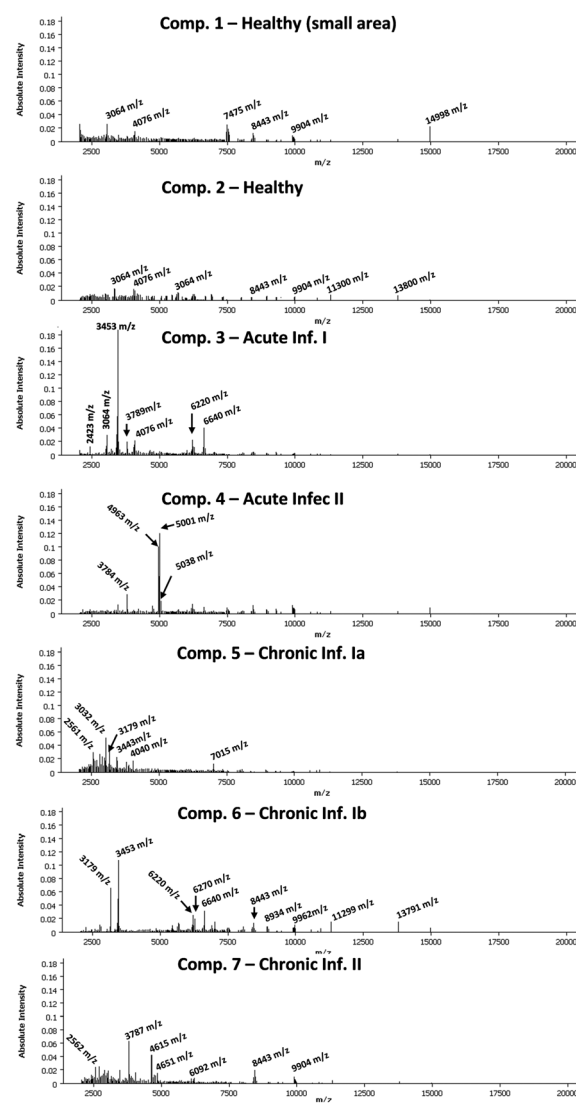

Fig. 4 pLSA loading plots interpreted as mass spectra specific for each phase, which we called healthy; acute infection I and II; and chronic infection Ia, Ib and II.
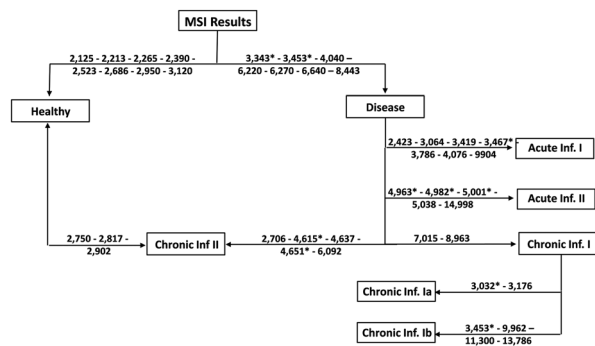
Fig. 5 Decision tree classification for visceral leishmaniasis stages using MALDI MSI. The results of the spectra are screened for the higher intensity/absence/presence of a limited number of infection phase identifying mass peaks. The major infection phase identifying biomarker ions are indicated by asterisks. Ions with an AUC above 0.7 were used to build the decision tree classification.

Fig. 6 MALDI-MSI showing the co-localization of the ions of m/z 4963 and 6620 with correlations > 0.8.

important changes in the protein profile during each phase of infection, named in this work as healthy, acute infection and chronic infection.

Visual inspection of the pLSA loading mass spectra reveals that the majority of the ion peak intensities show an increment or reduction according to the phase. Aiming at the classification of each phase, further analysis of these ions was performed by a hierarchical decision tree network-like approach (Fig. 5). It consists of a sequential scanning of ions for the relative intensity of their ion peaks or their absence/presence displaying specificities at different phase levels. Discrimination ability was determined by the receiver operating characteristic (ROC) curve analyzing data subsets composed of multiple MALDI-MS data obtained from each region defined by a segmentation map. The calculation of the ROC curve for a specific m/z value involves estimating sensitivity and specificity values for a trivial threshold classifier and then plotting a curve for the computed values. Typically, when two different regions were compared, not more than 8 potentially region/phase-discriminating ion peaks per spectrum were observed, of which usually several were present in more than one region. Each ion was therefore carefully inspected for a phase-identifying biomarker and combinations thereof. The area under the ROC curve (AUC value) assumes values between 0 and 1 and expresses the discrimination power of the m/z signal in one value, where the closer the AUC to 0.5, the less useful the m/z value. Promising markers displaying values above 0.7 were selected and evaluated for their usage to discriminate either a single region or phase of infection (data not shown).

Following the segmentation map and pLSA, the dendrogram in Fig. 5 discriminates uninfected and infected tissues, named as "Healthy" and "Disease" clades, respectively. In addition, the decision tree can point out the ions responsible for this discrimination. The ions of m/z 3343 and 3453 are characteristic for the disease clade, suggesting the participation of the respective biomolecules in the host response against the parasite. Interestingly, the ions of m/z 3467, 4963, 4982, and 5001 differentiate the acute infection phase, indicating different molecular processes in this period.
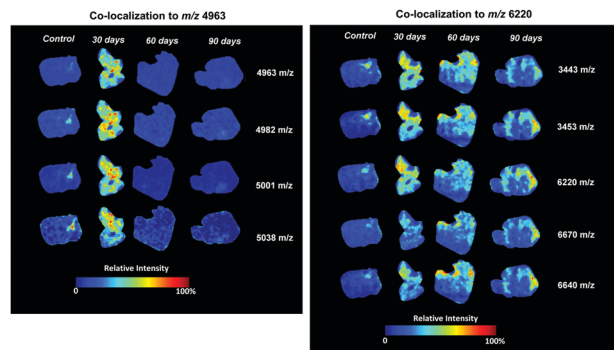
Note that large hepatomegaly and a high number of amastigotes were detected in the liver 30 days p.i. (Fig. 1), corroborating with this hypothesis. The tissues at 60 and 90 days p.i. show a spectral profile very similar to the one from uninfected tissue, demonstrated by the connection between the "healthy" and "chronic infection II" clades. Again, the liver weight decreases after 30 days p.i., corroborating with a different pathological physiological mechanism during the chronic infection stage. The total number of parasites decreases, however, only at 90 days p.i., indicating that the biomolecules associated with the ions of m/z 4615 and 4651 are overexpressed when the disease is in an advanced stage.

Variable expression rates of the proteins due to differential regulation per biological state in each phase might be observed, possibly leading to false negatives when the protein concentration is below the detection limit or the peak expression is in transition between 2 regions. For chronic infection Ia and Ib, the spectral data are close, indicating a change of the biological state or a transition to chronic infection II, which is the phase more correlated to the healthy area (see the dendrogram). For example, the ions of m/z 2750, 2817 and 2902 are not used as discriminating ions since their peak intensities are higher in both healthy and chronic stages. Such ions might represent the content of cell debris due to necrosis. The content of hepatocytes is exposed during necrosis and parasite load tends to be less intense in terms of proportion. This trend may explain the similarity between healthy and advanced infections. The ions of m/z 3443, 3453, 6220, 6270 and 6640 are disease-discriminating and were spread in the liver during the whole disease progression time and are not able to discriminate any progress of the disease. This spreading seems to indicate an overexpression of these peptides/proteins in the liver during any leishmaniasis phases induced by *L. infantum*. Fig. 6 demonstrates how these ions are co-localized in the tissue.

The significance of the marker ions and their origin

Aiming to confirm whether the prominent ions in MALDI-MS imaging were provided by the parasite presence in the liver, we compared the mass spectra of (a) *L. infantum* amastigotes cultured *in vitro*, (b) cultured J774 murine macrophages, (c) J774 murine macrophages infected by *L. infantum*, and (d) healthy

tissue and infected tissue at (e) 30 days and (f) 60 days p.i. (Fig. S2, ESI†). The protein ions observed in isolated amastigotes did not correspondent to any infected tissue peak, suggesting that the changes in protein fingerprinting observed in the liver during visceral leishmaniasis are unrelated to the parasite itself. Indeed detection of *L. infantum* ions/proteins is not expected in the liver MALDI-MSI since the estimated amount of parasite proteins present in the liver is very low compared with the amount of hepatic proteins: 2–6 × 10⁶ amastigotes (total protein content is around 15 μg) *versus* 135 × 10⁶ hepatic cells (total protein content is around 270 mg) per infected liver.[34]

Since macrophages act as both host cells for *Leishmania* and as an inductor of the immune responses,[10] a massive presence of these cells is expected in the infected tissues during visceral leishmaniasis. The ions detected in the infected macrophages culture and in the infected tissue might therefore correspond to the same protein or peptides. The ions of *m/z* 4963 and 6220 are prominent in both uninfected and infected macrophage *in vitro* cultures as well as in the infected livers. The ion of *m/z* 4963 is specially highlighted at 30 days p.i. as a marker for acute infection II, whereas it is insignificant in the uninfected liver, and the livers at 60 and 90 days p.i. Interestingly, we have detected co-localization[26] with a correlation threshold above 0.8 (Fig. 6) for the ions of *m/z* 4963, 4985, 5001 and 5038 respectively, which we suggest to be sodium [M + Na]⁺ and potassium [M + K]⁺ adducts. Na and K salts are very abundant electrolytes in the liver with significant alterations due to pathophysiological conditions[35] or also some protein isoforms. At the region named acute infection I, the ion of *m/z* 4963 presents a reduction of its relative peak intensity suggesting a decrease in the number of macrophages and a change in the cell population, which is demonstrated by the intensity boxplot (Fig. S3, ESI†). This change might be related to progression to the chronic condition. The discriminant ability of the selected ions in the infected liver seems not to be related to the presence of the parasite *per se*, but most likely corresponds to the immune or inflammatory response of the host against *L. infantum* infection. The multiple change in peptide/protein abundance during disease progression could therefore be a new source of candidate biomarkers.

Protein identification and biological comments

A search by *m/z* values in the MSiMass List database, which is a list of proteins reported from MALDI-MS imaging,[36] allowed the ion of *m/z* 4963 to be tentatively assigned to the Thymosin β4 protein with an error as low as 2 Da.[37] The ions of *m/z* 4986 and 5001 have a high correlation distribution (co-localization) with the ion of *m/z* 4963, and might be related either to [M + Na]⁺ or [M + K]⁺ adducts or Thymosin β4 isoforms. Corroborating this assignment, shotgun proteomics analysis of the infected mouse livers detected Thymosin β4, which is a ubiquitous peptide with a sequence of 40–44 amino acid residues that plays an important role in angiogenesis.[38] Recent evidence indicates that Thymosin β4 is upregulated in human livers with advanced fibrosis and mouse livers with chronic damage[38,39] and exogenous Thymosin β4 treatment ameliorates the liver damage in mice.[40] We found no

reports of its expression or function during leishmaniasis but speculate that the peptide is present due to the liver injuries caused by *Leishmania* infection and could function as an anti-inflammatory or anti-fibrotic agent to improve liver function. Our data indicate therefore a relationship of this peptide with the acute infection stage, and the hypothesis that Thymosin β4 plays an important role in leishmaniasis should be further investigated.

In this initial study, other highlighted ions by the mentioned database could not be assigned, perhaps due to the absence of reports focused on the mouse liver. If this bridge is constructed, then a relationship with data observed in MALDI MSI with protein sequencing by shotgun proteomics would be established. Detailed experiments with electrophoresis protein purification and/or top-down experiments are necessary to identify these important ions for visceral leishmaniasis. Our research group is currently working on these identifications.

Conclusions

Visceral leishmaniasis progression in a mouse model was for the first time studied by MALDI MSI, and indeed this technique showed strong potential as a new tool in this field. It revealed key biochemical modifications with regard to proteins or peptides on *Leishmania* infection which could not be detected by microscopic analysis. Statistical analysis of the MSI data could divide *Leishmania* infection into 3 stages, namely heathy, acute infection and chronic infection. All spectral features detected by statistical tools corroborate with micro- and macroscopic observations, supporting the hypothesis of different molecular events during disease progression. We have identified some potential ions associated with biomarker candidates to study the disease progress. Among the 8 statistically highlighted ions, that of *m/z* 4963 was identified as Thymosin β4 and those of *m/z* 4986 and 5001 were identified as adducts of this peptide or its isoforms. Thymosin β4 was previously related to liver damage and recovery in humans, and seems to be involved in the acute infection response of mice against *Leishmania* infection. Further studies focusing on the identification of the remaining ions are in progress in our group.

The MALDI MSI approach used herein combined screening for unknown molecules, associations with the infected tissue and important molecular features, enabling prioritization of specific ions for subsequent identification. It is intuitive that these ions with the strongest pathological associations may be relevant and biologically interesting. The numerical data (*m/z* values of ion peaks) generated here are easy to be exchanged between laboratories which are focused on leishmaniasis studies and to be explored by other laboratories dedicated to understanding this neglected tropical disease. After characterization of the ions in question, such data would have high likelihood to diagnostic applications. Whereas several biological questions about the complex *Leishmania* host interaction, immune responses, visceralization and persistence processes are still to be answered, this report strongly indicates that MALDI MSI can complement microscopic analysis and classical

imaging techniques with a detailed molecular view of the biochemistry in progress.

Acknowledgements

References

1 M. M. Gessel, J. L. Norris and R. M. Caprioli, *J. Proteomics*, 2014, **107**, 71–82.

2 E. H. Seeley and R. M. Caprioli, *Trends Biotechnol.*, 2011, **29**, 136–143.

3 K. Schwamborn and R. M. Caprioli, *Mol. Oncol.*, 2010, **4**, 529–538.

4 E. A. Jones, S. O. Deininger, P. C. Hogendoorn, A. M. Deelder and L. A. McDonnell, *J. Proteomics*, 2012, **75**, 4962–4989.

5 H. E. Hulme, L. M. Meikle, H. Wessel, N. Strittmatter, J. Swales, C. Thomson, A. Nilsson, R. J. B. Nibbs, S. Milling and P. E. Andren, *Sci. Rep.*, 2017, **7**, 2786.

6 A. S. Attia, K. A. Schroeder, E. H. Seeley, K. J. Wilson, N. D. Hammer, D. C. Colvin, M. L. Manier, J. J. Nicklay, K. L. Rose and J. C. Gore, *Cell Host Microbe*, 2012, **11**, 664–673.

7 X. Xie, Y. Jiang, Y. Yuan, P. Wang, X. Li, F. Chen, C. Sun, H. Zhao, X. Zeng and L. Jiang, *Oncotarget*, 2016, **7**, 59987.

8 C. Zhang, G. Arentz, L. Winderbaum, N. A. Lokman, M. Klingler-Hoffmann, P. Mittal, C. Carter, M. K. Oehler and P. Hoffmann, *Int. J. Mol. Sci.*, 2016, **17**, 1088.

9 J. L. Moore, K. W. Becker, J. J. Nicklay, K. L. Boyd, E. P. Skaar and R. M. Caprioli, *Proteomics*, 2014, **14**, 820–828.

10 G. A. Duque and A. Descoteaux, *Curr. Opin. Microbiol.*, 2015, **26**, 32–40.

11 N. K. Copeland and N. E. Aronson, *Curr. Opin. Infect. Dis.*, 2015, **28**, 426–437.

12 M. E. Wilson, S. M. B. Jeronimo and R. D. Pearson, *Microb. Pathog.*, 2005, **38**, 147–160.

13 M. Podaliri Vulpiani, L. Iannetti, D. Paganico, F. Iannino and N. Ferri, *Vet. Med. Int.*, 2011, **2011**, 215964.

14 D. Pace, *J. Infect.*, 2014, **69**, S10–S18.

15 R. J. Faleiro, R. Kumar, L. M. Hafner and C. R. Engwerda, *PLoS Neglected Trop. Dis.*, 2014, **8**, e2914.

16 A. Nieto, G. Domínguez-Bernal, J. A. Orden, R. De La Fuente, N. Madrid-Elena and J. Carrión, *Vet. Res.*, 2011, **42**, 39.

17 C. Cassagne, F. Pratlong, F. Jeddi, R. Benikhlef, K. Aoun, A. C. Normand, F. Faraut, P. Bastien and R. Piarroux, *Clin. Microbiol. Infect.*, 2014, **20**, 551–557.

18 L. Beattie and P. M. Kaye, *Cell. Microbiol.*, 2011, **13**, 1659–1667.

19 I. Grekov, M. Svobodová, E. Nohýnková and M. Lipoldová, *J. Microbiol. Methods*, 2011, **87**, 273–277.

20 T. Alexandrov, M. Becker, S.-O. Deininger, G. n. Ernst, L. Wehder, M. Grasmair, F. von Eggeling, H. Thiele and P. Maass, *J. Proteome Res.*, 2010, **9**, 6535–6546.

21 S. Rauser, S.-O. Deininger, D. Suckau, H. Höfler and A. Walch, *Expert Rev. Proteomics*, 2010, **7**, 927–941.

22 S. Rauser, C. Marquardt, B. Balluff, S. r.-O. Deininger, C. Albers, E. Belau, R. Hartmer, D. Suckau, K. Specht and M. P. Ebert, *J. Proteome Res.*, 2010, **9**, 1854–1863.

23 N. Poté, T. Alexandrov, J. Le Faouder, S. Laouirem, T. Léger, M. Mebarki, J. Belghiti, J. M. Camadro, P. Bedossa and V. Paradis, *Hepatology*, 2013, **58**, 983–994.

24 O. Klein, K. Strohschein, G. Nebrich, J. Oetjen, D. Trede, H. Thiele, T. Alexandrov, P. Giavalisco, G. N. Duda and P. von Roth, *Proteomics*, 2014, **14**, 2249–2260.

25 T. Alexandrov, *BMC Bioinf.*, 2012, **13**, S11.

26 L. A. McDonnell, A. van Remoortere, R. J. M. van Zeijl and A. M. Deelder, *J. Proteome Res.*, 2008, **7**, 3619–3627.

27 N. Rolão, C. Melo and L. Campino, *Acta Trop.*, 2004, **90**, 123–126.

28 J. Carrion, A. Nieto, S. Iborra, V. Iniesta, M. Soto, C. Folgueira, D. R. Abanades, J. M. Requena and C. Alonso, *Parasite Immunol.*, 2006, **28**, 173–183.

29 T. Alexandrov, S. Meding, D. Trede, J. H. Kobarg, B. Balluff, A. Walch, H. Thiele and P. Maass, *J. Proteomics*, 2011, **75**, 237–245.

30 T. Hofmann, Presented in part at the Proceedings of the 22nd annual international ACM SIGIR conference on Research and development in information retrieval, Berkeley, California, USA, 1999.

31 S.-O. Deininger, M. Becker and D. Suckau, *Mass Spectrometry Imaging: Principles and Protocols*, 2010, 385–403.

32 M. Hanselmann, M. Kirchner, B. Y. Renard, E. R. Amstalden, K. Glunde, R. M. A. Heeren and F. A. Hamprecht, *Anal. Chem.*, 2008, **80**, 9649–9658.

33 H. Akaike, *IEEE Trans. Autom. Control*, 1974, **19**, 716–723.

34 A.-K. Sohlenius-Sternbeck, *Toxicol. in Vitro*, 2006, **20**, 1582–1586.

35 J. H. Atterhög, B. HåKansson, S. A. Johansson and I. G. Porjé, *J. Intern. Med.*, 1964, **175**, 251–255.

36 L. A. McDonnell, A. Walch, M. Stoeckli and G. L. Corthals, *J. Proteome Res.*, 2013, **13**, 1138–1142.

37 S. M. J. Rahman, A. L. Gonzalez, M. Li, E. H. Seeley, L. J. Zimmerman, X. J. Zhang, M. L. Manier, S. J. Olson, R. N. Shah, A. N. Miller, J. B. Putnam, Y. E. Miller, W. A. Franklin, W. J. Blot, D. P. Carbone, Y. Shyr, R. M. Caprioli and P. P. Massion, *Cancer Res.*, 2011, **71**, 3009–3017.

38 J. Kim, S. Wang, J. Hyun, S. S. Choi, H. Cha, M. Ock and Y. Jung, *PLoS One*, 2015, **10**, e0122758.

39 S. Nemolato, P. Van Eyken, T. Cabras, F. Cau, M. U. Fanari, A. Locci, D. Fanni, C. L. P. Gerosa, I. Messana and M. Castagnola, *Eur. J. Histochem.*, 2011, **55**, 25.

40 K. Reyes-Gordillo, R. Shah, J. Arellanes-Robledo, M. Rojkind and M. R. Lakshman, *Ann. N. Y. Acad. Sci.*, 2012, **1269**, 61–68.